Toxicology Research

RSC Publishing

PAPER

View Article Online
View Journal | View Issue

Cite this: *Toxicol. Res.*, 2013, **2**, 270

Corona protein composition and cytotoxicity evaluation of ultra-small zeolites synthesized from template free precursor suspensions†

S. Laurent,‡[a] E.-P. Ng,‡[b] C. Thirifays,[a] L. Lakiss,[c] G.-M. Goupil,[c] S. Mintova,*[c] C. Burtea,[a] E. Oveisi,[d,e] C. Hébert,[d,e] M. de Vries,[f] M. M. Motazacker,[g] F. Rezaee§*[f] and M. Mahmoudi§*[h,i]

The toxicity of two types of ultra-small zeolites (8–18 nm) with LTL- and EMT-type structures is reported. Both the LTL- and EMT-type zeolites belong to the same group of molecular sieves; they have large pores (7.1–7.5 Å) and low silica content (Si/Al = 1.2–2.3). The zeolites are prepared by an environmentally friendly synthetic approach from precursor suspensions without using any organic template. Cellular interactions with the two types of zeolite nanocrystals are evaluated by cell viability, reactive oxygen species and cell life cycle assays. It is found that various concentrations of zeolites have negligible effects on the cell life cycle. Moreover, the LTL- and EMT-types zeolites did not cause extensive oxidative stress on the cells. Although it is seen that the zeolites extensively entered in the cells, there is no sign of toxicity for all employed concentrations of ultra-small EMT and LTL zeolites. Additionally, no abnormality in DNA replication while exposed to the zeolites is observed. Very importantly, the zeolite corona shows a high affinity for fibrinogen, moderate affinity for apoA-II and complement factor 3, and trace affinity for albumin, which is the most abundant protein of human plasma. Thus the zeolite nanoparticles can be considered as very promising material for purification of fibrinogen and lipoproteins. Since fibrinogen is considered as acute phase protein and found to be the most associated biomolecule in the composition of corona at the surface of zeolites, we propose that these nanoparticles can be potentially pro-inflammatory for *in vivo* applications.

Received 22nd February 2013,
Accepted 24th April 2013

DOI: 10.1039/c3tx50023c

www.rsc.org/toxicology

Introduction

Zeolites are metastable crystalline aluminosilicate molecular sieves with uniform pores of molecular dimensions that are widely applied in catalysis, separation and adsorption.[1] Subdivision of zeolite crystals into nanometer scale has potentially expanded their applications towards electronic devices, host–guest systems, drug delivery, optical coatings, sensors and energy conversion due to their small particle size, short diffusion pathway, large external surface area, defined porosity and controllable surface properties.[2,3]

With the further development of zeolite chemistry, more structures are synthesized and the new technologies allow a great control of crystal size, pore size, morphology, acidity, porosity, *etc.* In addition, the new developments in zeolite synthesis are expected to broaden their applications in the fields of green chemistry, medicine, nanotechnology, pharmaceuticals, and the food industry. Therefore information on the toxicity of the zeolite particles is a primary need prior their applications.

In general, nanosized zeolites display different physicochemical properties than micron-sized zeolites. While micron-sized zeolites are considered as non-toxic and environmentally

[a]*Department of General, Organic, and Biomedical Chemistry, NMR and Molecular Imaging Laboratory, University of Mons, Avenue Maistriau, 19, B-7000 Mons, Belgium*
[b]*School of Chemical Sciences, Universiti Sains Malaysia, 11800 USM, Penang, Malaysia*
[c]*Laboratory of Catalysis and Spectroscopy, ENSICAEN, University of Caen, CNRS, 6 Boulevard du Maréchal Juin, 14050 Caen, France. E-mail: mintova@ensicaen.fr*
[d]*Interdisciplinary Centre for Electron Microscopy, École Polytechnique Fédérale de Lausanne (EPFL), CH-1015 Lausanne, Switzerland*
[e]*Electron Spectrometry and Microscopy Laboratory, École Polytechnique Fédérale de Lausanne (EPFL), CH-1015 Lausanne, Switzerland*
[f]*Department of Cell Biology, University Medical Center Groningen, University of Groningen, Groningen, The Netherlands. E-mail: f.rezaee@med.umcg.nl*
[g]*Department of Experimental Vascular Medicine, Academic Medical Center, Amsterdam, The Netherlands*
[h]*Department of Nanotechnology, Faculty of Pharmacy, Tehran University of Medical Sciences, Tehran, Iran. E-mail: Mahmoudi@illinois.edu*
[i]*Nanotechnology Research Center, Faculty of Pharmacy, Tehran University of Medical Sciences, Tehran, Iran*

†Electronic supplementary information (ESI) available. See DOI: 10.1039/c3tx50023c

‡These authors contributed equally to this work as first author.

§These authors contributed equally to this work as last author.

benign, attention has very seldom been paid to health and safety issues of nanosized zeolites.[4] Thus, cytotoxicity evaluation of inorganic nanoparticles such as zeolites, metals and metal oxides has been gradually recognized as a crucial issue in "nanosociety".[5,6] This is because these nanoparticles have a possible adverse effect on human health compared to their micrometer counterparts. The human body is exposed to inorganic nanoparticles through various routes including inhalation, skin contact, ingestion and injection.[7] Thus, cytotoxicity has been gaining increased attention for the purpose of the establishment of nano-safety regulations.

Several articles reported on the toxicity of nanosized zeolites (A,[8,9] Y,[8] ZSM-5,[9] silicalite,[9,10] LTL[9]). For instance, Thomassen and his co-workers performed *in vitro* cytotoxicity experiments on colloidal zeolites A and Y synthesized in the presence of organic templates with particle sizes of 25–100 nm using macrophages, epithelial and endothelial cells by determining mitochondrial activity (MTT assay) and cell membrane integrity (LDH leakage assay).[8] The nano-sized zeolites showed low toxicity to the cells. Kihara *et al.*[9] and Petushkov *et al.*[10] investigated the toxicities of nanosized zeolites A, ZSM-5 and silicalite-1 synthesized with organic templates and template free LTL (30–500 nm) using human embryonic kidney 293 (HEK-293), RAW264.7 macrophage and HeLa cells. The toxicities of zeolite nanoparticles were found to be dependent on their size, Si/Al ratio and shape. Pure siliceous MFI-type zeolite (silicalite-1) is not toxic, but the other three aluminum-containing nanosized zeolites show a dose-dependent toxic manner.

Certain nanosized molecular sieves have been obtained at moderate (60–130 °C) and low (<60 °C) temperatures.[11–15] Low temperature synthetic techniques for discrete zeolite nanocrystals from organic free precursor systems are highly desired, as they would reduce cost and hazardous wastes, save energy and possibly alter the properties of the materials.[3,16] Therefore here we study the toxicity of two types of ultra-small zeolites with LTL- and EMT-type structures synthesized from template free $Na(K)_2O$–Al_2O_3–SiO_2–H_2O precursor systems, *i.e.*, from K- and Na-rich precursor suspensions, respectively. Cellular interactions with the zeolite nanocrystals are evaluated by several methods such as cell viability, reactive oxygen species, and cell life cycle assays. The template free ultra-small LTL- and EMT-type zeolites are prepared by an environmentally friendly approach, which is directly linked to decreasing amounts of hazardous residues and with a special attention to the environmental, health and safety issues.

Experimental section

Preparation of ultra-small zeolites free of templates

The nanosized EMT-type zeolite, with size of 8–18 nm, was synthesized from a clear precursor suspension with the molar composition $18.45Na_2O : 5.15SiO_2 : 1Al_2O_3 : 240.3H_2O$.[14] The samples were treated at 30 °C for 36 hours.

The nanosized LTL-type zeolite (8–18 nm) was synthesized from a clear precursor suspension with the molar composition $5K_2O : 10SiO_2 : 0.5Al_2O_3 : 200H_2O$.[15] The suspension was heated in a microwave oven at 170 °C (800 W) for 10 min or in a conventional oven at 170 °C for 48 hours.

Prior to characterization, the LTL and EMT nanosized crystals were purified by high speed centrifugation (25 000 rpm for 3 hours) and re-dispersed in doubly distilled water; this procedure was repeated 5 times until the final colloidal suspensions have a pH of 7.5 and solid concentration of particles of 5 wt%.

General characterization

The structures of the EMT and LTL nanosized crystals were determined by X-ray diffraction (XRD) measurements using a PANalytical X'Pert Pro diffractometer in Debye–Scherrer geometry with Cu Kα radiation (λ = 1.5418 Å). The particle diameter of the as-synthesized zeolite crystals was determined by dynamic light scattering (DLS) with a Malvern Zetasizer-Nano instrument. In order to probe the size and crystal structure of the particles, transmission electron microscopy (TEM) was employed. For TEM analysis, colloidal suspensions of EMT and LTL crystals were dried on copper grids and studied using a FEI Tecnai F20 operating at 200 kV.

The chemical compositions of the nanocrystals were determined by X-ray fluorescence (XRF) spectroscopy using a MagiX PHILIPS PW2540. In addition, nitrogen adsorption–desorption isotherms were measured using a Micromeritics ASAP 2010 volumetric adsorption analyzer. Samples were dehydrated at 250 °C under vacuum overnight prior to the measurements. The external surface area and micropore volume were estimated using *t*-plots, and the micro- and mesopore size distributions of the EMT and LTL samples were estimated by the Density Functional Theory (DFT) and Barret–Joyner–Halenda (BJH) methods, respectively.

Preparation of surface saturated zeolites

The EMT- and LTL-type zeolites were incubated with cell medium for 24 hours (without cells). After the incubation, the particles were collected, using centrifugation (1 hour at 24 000 rpm), and redispersed in fresh PBS.

Cell culture and treatments

HeLa (human cervical adenocarcinoma) cells were cultured in RPMI culture medium supplemented with 10% fetal bovine serum and 1% Pen Strep (all from Gibco).

Cell viability

The viability of HeLa cells in response to the incubation with zeolites was determined with the Cell Titer-Glo-Assay Luminescent Cell Viability Assay. 10 000 HeLa cells were seeded into 96-well plates and cultivated overnight. After intensive washing, the cells were incubated with culture medium and zeolites (100 μg ml^{-1}) for 6 hours. 100 μl of Cell Titer-Glo reagent per well was added and the plates were shaken (orbital) for 2 minutes. After incubation (10 minutes) at room

temperature, the luminescence was measured with a plate reader Infinite M200.

Reactive oxygen species (ROS) assay

For the determination of intracellular ROS levels, the fluorescent dye 2′,7′-dichlorodihydrofluorescein diacetate (H_2DCF-DA) (Invitrogen, USA) was used.[17] In the presence of intracellular esterases this nonpolar component is converted into the non-fluorescent polar derivative H_2DCF. This intermediate is membrane impermeable and rapidly oxidized to fluorescent 2′,7-dichlorofluorescein (DCF) by ROS. The cells were seeded in 96-well plates overnight. Cells were incubated with the zeolites (100 μg ml^{-1}) for 6 hours, and 50 μM H_2DCF-DA was added. After 30 minutes the intracellular DCF fluorescence was measured with a plate reader infinite M200 (Tecan) with an excitation wavelength of 485 nm. Emission was recorded at 535 nm (all data were corrected for background fluorescence).

For visualization of the ROS, confocal microscopy was employed. The HeLa cells were seeded on cover slips before incubation with various compounds. The cells were incubated for 24 h with a zeolite concentration of 100 μg ml^{-1}. Control cells were not incubated with zeolite. The cells were then washed once with PBS and twice with Hanks Buffered Salt Solution (HBSS). The cells were incubated for 45 minutes with H_2DCFDA 25 μM in HBSS at 37 °C. Then, 1.5 μl of Hoechst solution was added and the cells were incubated for 5 minutes at 37 °C. After washing, the cell-coated cover slips were mounted in HBSS on microscope slides.[18]

Lysosome labeling

HeLa cells were labeled with the Image-iT™ LIVE lysosomal and nuclear labeling kit (Molecular Probes, Invitrogen), which provides a red fluorescent LysoTracker® Red DND-99 dye for lysosome staining and a blue fluorescent Hoechst 33342 dye for staining the nucleus. The cells were seeded on cover slips and were incubated (37 °C, 24 hours) with zeolite crystals added to the culture medium at a concentration of 200 μg ml^{-1} (control cells were not incubated with the nanoparticles). After rinsing the cells with HBSS, they were labeled with the Image-iT™ LIVE lysosomal and nuclear labeling kit according to the supplier's instructions. Briefly, the cells were incubated for 5 minutes with 2 μg ml^{-1} of Hoechst 33342 solution, followed by incubation with 100 nM of LysoTracker Red DND-99® for one minute. The cells were rinsed twice with HBSS after each dye treatment. The living cells were finally mounted in HBSS on microscope slides and observed on a DM2000 Leica microscope (Leica Microsystems, Groot Bijgaarden, Belgium); images were acquired with a Leica DFC 290 camera.

Cell cycle

The cell cycle assay was carried out by staining of the DNA with propidiumiodide (PI) followed by flow cytometric measurement of the fluorescence. Approximately 10^6 HeLa cells were maintained in culture after de-freezing, to retain their physiologic cell cycle distribution. After achieving 75% confluences they were treated with zeolite nanoparticles (concentration of 100 μg ml^{-1}) for 24 hours. The adhering cells were detached from the plates by trypsin + EDTA or EDTA alone (25 mg trypsin and 5 mg EDTA per 1 ml), and harvested. The obtained suspensions of adhering or floating cells were centrifuged at 280*g*. The collected cells were washed with PBS several times at 200*g*. Cells were fixed in ethanol *via* transferring into tubes containing 70% ethanol and stored at 20 °C for several days. Prior to the flow cytometric analysis, the ethanol suspended cells were centrifuged at 300 rpm for 5 minutes, and the supernatants were decanted thoroughly. The collected cells were washed with PBS and then suspended in 1 ml of PI/Triton X-100 staining solution with RNase A, and then kept at 37 °C for 30 minutes. The stained cells were then analyzed by flow cytometry using Cyflow SL machine (Partec, Germany) with excitation at 488 nm and collecting data at FL2. The readings were analyzed with Flowjo software (Treestar Inc., CA, USA).

Collection of plasma

Blood was drawn from healthy volunteers, and stored in tubes containing Na-citrate as anticoagulant. Subsequently, plasma was isolated by centrifugation at 1500*g* for 20 min at 4 °C and stored at −80 °C for further analysis.

Incubation of ultra-small LTL and EMT zeolites with 10% and 100% human plasma

LTL and EMT nanosized zeolites were exposed to 10% and 100% human plasma and incubated for 1 hour at room temperature; these samples are named LTL-10, LTL-100 and EMT-10 and EMT-100. Thereafter, the zeolite crystals were centrifuged for 20 minutes at 10 000 rpm. Subsequently, the supernatants were carefully removed without touching the pellet consisting of zeolite particles and washed with PBS. This step was repeated 5 times. Finally the particles were speed-vacuumed for drying. Then, the LTL- and EMT-corona associated proteins were reduced with DTT to breakdown disulfide bridges and in turn cut with trypsin to generate peptides. Finally the extracted peptides were dried in the speed-vacuum and subsequently redispersed in 30 μl Milli-Q water containing 0.5% formic acid. Then each sample was run 3 or 4 times by nLC-MS/MS (3 μl of each fraction was injected into nLC-MS/MS, LTQ-ORBITRAP-XL).[19]

LTQ Orbitrap XL characterization

Samples were analyzed by NanoLC-MS/MS on an Ultimate 3000 system (Dionex, Amsterdam, The Netherlands) interfaced online with a LTQ Orbitrap XL mass spectrometer (Thermo Fisher Scientific, San Jose, CA). Re-dissolved peptides were loaded onto a 5 mm × 300 μm i.d. trapping micro column packed with C18 PepMAP100 5 μm particles (Dionex) in 0.1% FA at the flow rate of 20 μL min^{-1}. Upon loading and washing, peptides were back-flush eluted onto a 15 cm × 75 μm i.d. nano-column, packed with C18 PepMAP100 3 μm particles (Dionex).[19] The following mobile phase gradient was delivered at the flow rate of 300 nL min^{-1}: 5–50% of solvent B in 93 minutes; 50–80% B in 5 minutes; 80% B for 10 minutes,

and back to 5% B in 5 minutes. Solvent A was 100 : 0 H_2O–acetonitrile (v/v) with 0.1% formic acid, and solvent B was 10 : 90 H_2O–acetonitrile (v/v) with 0.1% formic acid. Peptides were infused into the mass spectrometer *via* a dynamic nanospray probe (Thermo Electron Corp.) with a stainless steel emitter (Proxeon, Odense, DK). The typical spray voltage was 1.6 kV with no sheath and auxiliary gas flow; the ion transfer tube temperature was 200 °C. The mass spectrometer was operated in data-dependent mode. The automated gain control (AGC) was set to 5×10^5 charges and 1×10^4 charges for MS/MS at the linear ion trap analyzer. The DDA cycle consisted of the survey scan within m/z 300–1300 at the orbitrap analyzer with target mass resolution of 60 000 (FWHM, full width at half maximum at m/z 400) followed by MS/MS fragmentation of the five most intense precursor ions under the relative collision energy of 35% in the linear trap. Singly charged ions were excluded from MS/MS experiments, and m/z of fragmented precursor ions were dynamically excluded for a further 90 s. The ion selection threshold for triggering MS/MS experiments was set to 500 counts. An activation parameter q of 0.25 and an activation time of 30 ms were applied.

Software

The recently developed software PEAKS DB (version 5.3) by Zhang *et al.*[20] was applied to the spectra generated by LTQ Orbitrap XL to screen the protein composition of corona of LTL- and EMT-type zeolites. The false discovery rate was manually adjusted into zero. The number of spectra per protein was also determined by PEAKS to calculate the $NpSpC_k$ value.

Results and discussion

General characterization of ultra-small EMT and LTL zeolites

The ultra-small zeolite crystals obtained under hydrothermal treatment of aluminosilicate precursor suspensions free of organic templates were isolated by high-speed centrifugation and freeze dried prior to characterization. The powder samples are entirely X-ray crystalline and display Bragg reflections corresponding to the EMT- and LTL-type zeolite structures. The sizes of these ultra-small EMT and LTL crystals were determined by dynamic light scattering (DLS). The particle size distribution (PSD) of the zeolites was measured in water suspensions with a constant solid concentration of 5 wt% and at a pH of 7.5. As shown in Fig. 1, the hydrodynamic diameter of the EMT and LTL crystals is about 8–18 nm. In addition, the morphology, size and crystalline features of the particles in both suspensions were verified by high-resolution transmission electron microscopy (HRTEM) (Fig. 2). The HRTEM images at high magnification reveal the presence of particles with an average diameter in the range of 8–18 nm having crystalline fringes corresponding to the EMT- and LTL-type structures (Fig. 2). The zeolites nanoparticles are very stable in doubly distilled water and their crystalline nature and mean size do not change with time as seen by DLS and HRTEM. In addition, the zeta potential determined by the electrophoretic

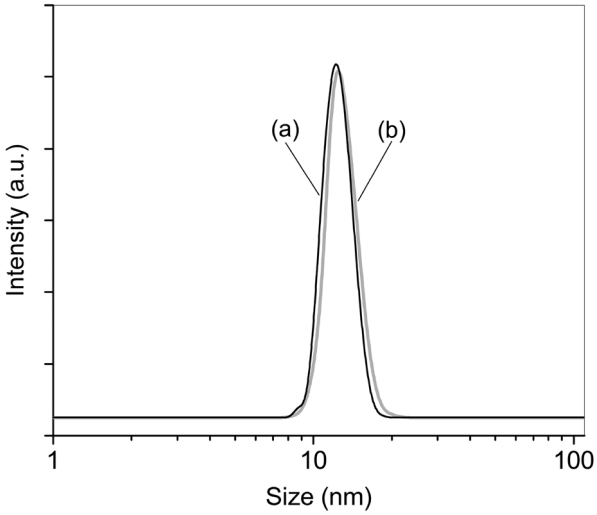

Fig. 1 DLS curves of ultra-small (a) EMT- and (b) LTL-type zeolites.

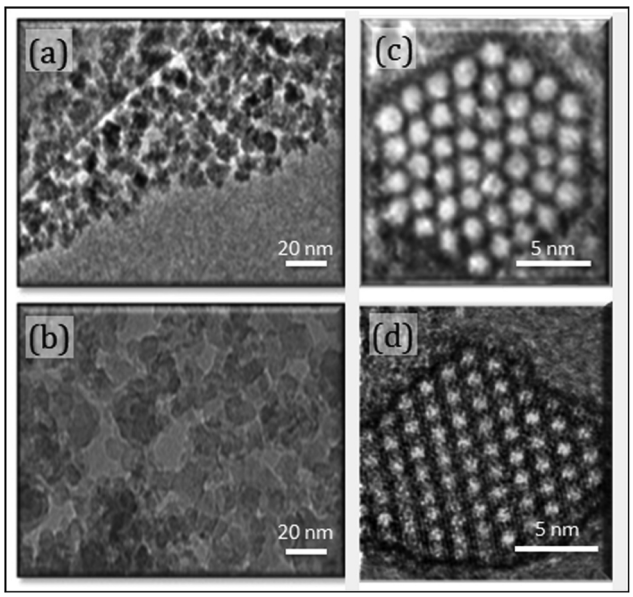

Fig. 2 TEM pictures of bulk (a) EMT and (b) LTL-type zeolites (M = 20 nm), and single (c) EMT and (d) LTL zeolite crystals (M = 5 nm).

mobility of both suspensions is lower than −35 mV. This confirms the stability of the negatively surface charged zeolite crystals in the water suspension with a neutral pH.[21] The conditions for the preparation and post-synthesis treatment (high speed purification and freeze drying) of nanosized zeolites allow preservation of single crystals with perfect hexagonal and almost spheroidal shapes for the EMT and LTL zeolites, respectively (Fig. 2c,d). Both zeolites contain channels in a highly ordered hexagonal arrangement. The EMT- and LTL-type zeolite crystals belong to the large pore molecular sieves with a pore size of 7.5 Å and 7.1 Å, respectively, as measured by nitrogen sorption. But due to the different framework type structures, the EMT and LTL zeolite nanosized crystals have three- and one-dimensional channel systems

(12-membered ring), respectively, which is schematically represented in Fig. 3B (see insert). Moreover, the different stacking of faujasite sheets creates two types of cages in the EMT-type zeolite, a hypocage (0.61 nm^3) and a hypercage (1.24 nm^3).[22] The structure of the LTL zeolite is based on polyhedral cages, which form columns running parallel to the *c* axis and thus provide one dimensional pores with a free diameter of 7.1 Å (see insert in Fig. 3B). In addition, the framework densities (FD) of the EMT- and LTL-type zeolites are 12.9 and 16.3, respectively. The FD, which is represented by the number of T-atoms per 1000 $Å^3$, is not only related to the pore volume of the zeolite but also depends on the chemical composition and flexibility of the skeleton structures. Since the EMT-type zeolite has much lower framework density, higher microporosity and flexibility for the crystallites are expected.

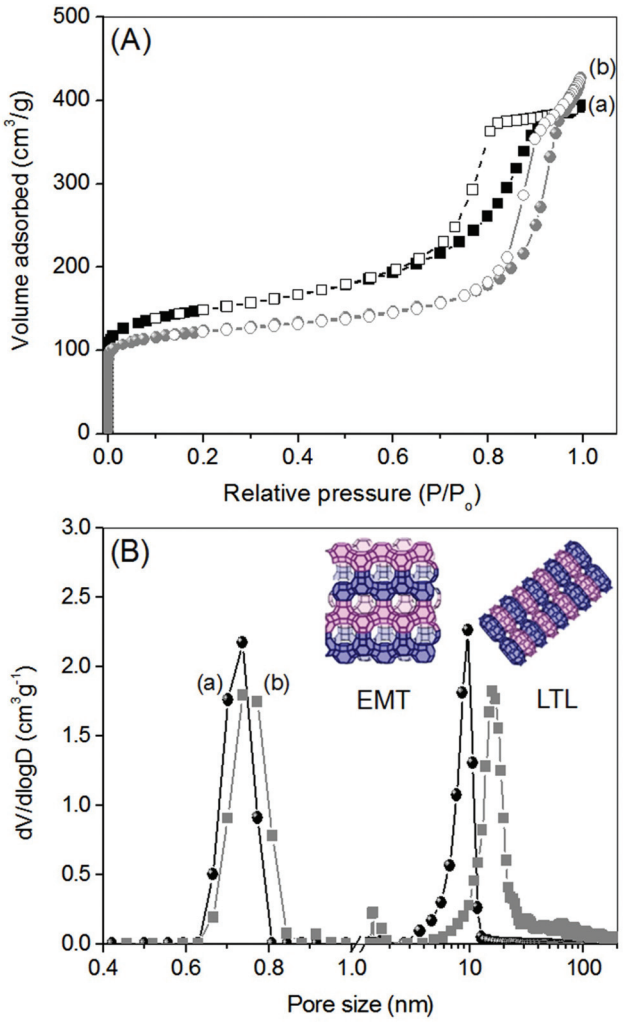

Fig. 3 (A) Nitrogen sorption isotherms and (B) pore (micro + meso) size distribution of ultra-small (a) EMT- and (b) LTL-type crystals. Insert in (B): schematic presentation of framework type of EMT- and LTL-type zeolites.

Therefore the EMT and LTL ultra-small zeolites were further characterized by nitrogen sorption measurements. The Type I sorption isotherms were measured for both samples, which reveal the presence of micropores (Fig. 3) and additional textural mesoporosity, which is attributed to the random packing of the ultra-small crystals (Fig. 3, Table 1). The Brunauer–Emmett–Teller (BET) surface area for the ultra-small EMT and LTL materials is 495 and 409 $m^2\ g^{-1}$, and the total pore volume is 0.60 and 0.64 $cm^3\ g^{-1}$, respectively, determined using non-porous Silica-1000 as a reference material (Table 1). The additional hysteresis loop at high partial pressure for both samples reveals the presence of mesopores in addition to the micropores typical for zeolites (Fig. 3B). Very narrow mesopores for both the EMT and LTL nanocrystals with a size of 10 and 16 nm, correspondingly, were measured. In conclusion, both zeolites have well developed micro- and mesoporosity, but different types of channels, *i.e.* the EMT and the LTL zeolites have three- and one-dimensional pore systems, respectively. Therefore fast diffusion within the EMT ultra-small crystals is expected.

Besides the different type of framework structures and size of micropores, the samples differ in chemical composition, *i.e.* the EMT zeolite has Si/Al ratio = 1.14 and Na/Al ratio = 0.92, while the LTL zeolite has Si/Al ratio = 2.60 and K/Al ratio = 1.14. The EMT nanocrystals have high aluminum and high sodium content, while the aluminum content in LTL is less, which is compensated by the presence of potassium cations. However, the EMT and LTL zeolite crystals belong to the same group of microporous materials, *i.e.*, both have large micropores (~7.3 Å) and they are low silica zeolites.

Toxicity measurements of ultra-small EMT and LTL zeolites free of organic templates

The interaction of human cells with zeolites was performed with a HeLa cell culture model under standard conditions. The results are shown in Fig. 4; the cell viability was not significantly affected after interaction with various concentrations of zeolites (50–400 μg ml^{-1}). However, the reduction of the detected cell viability for the EMT-type zeolite was stronger than for the LTL-type zeolite. It is well recognized that the protein corona would be formed at the surface of nanoparticles upon their entrance to the biological medium,[23–26] thus,

Table 1 Properties of LTL- and EMT-type zeolites

Samples	Si/Al ratio	S_{BET} ($m^2\ g^{-1}$)	$S_{external}$[a] ($m^2\ g^{-1}$)	$V_{micropore}$[a] ($cm^3\ g^{-1}$)	$V_{mesopore}$[a] ($cm^3\ g^{-1}$)	V_{total} ($cm^3\ g^{-1}$)	Mesopores (nm)	Mean particle size[b] (nm)
Ultra-small EMT	1.14	495	220	0.145	0.470	0.64	10	12
Ultra-small LTL	2.60	409	120	0.142	0.498	0.62	16	13

[a] Determined by DFT. [b] The particle size was determined by DLS and SEM/TEM techniques.

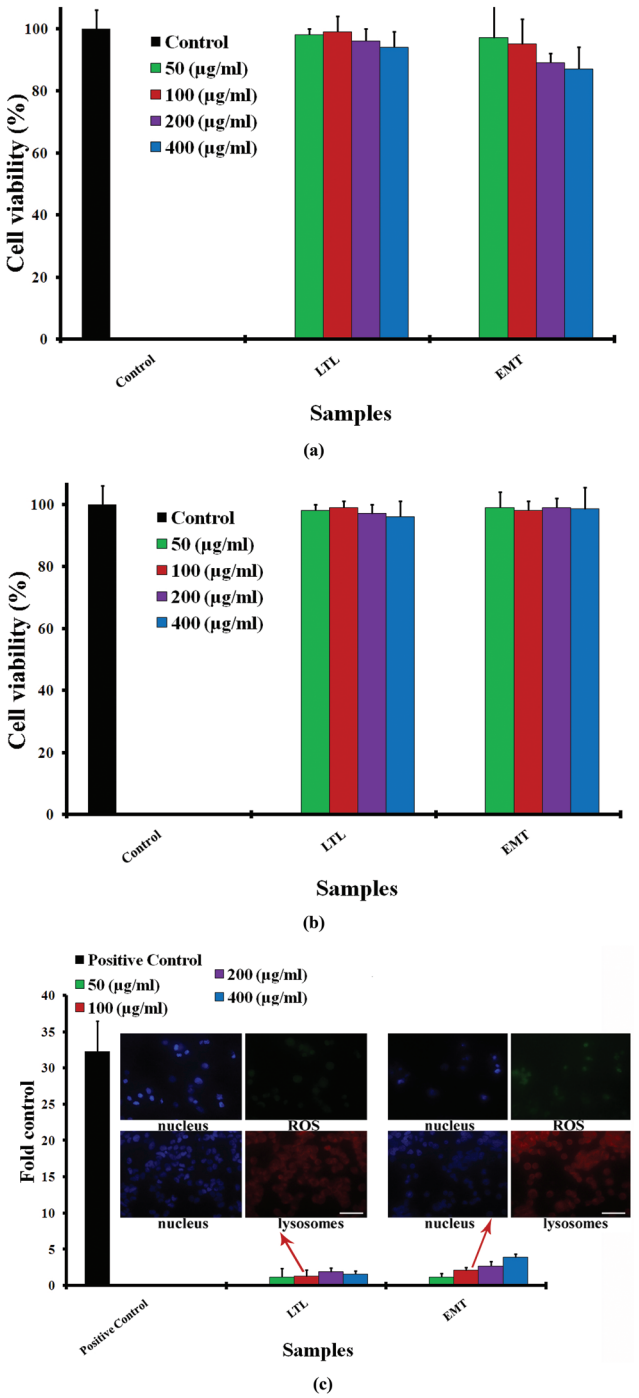

Fig. 4 (a) HeLa cell viabilities before and after interactions with various concentration of zeolites; (b) HeLa cell viabilities before and after interactions with various concentration of surface saturated zeolites; (c) ROS production for zeolites, at various concentrations (*i.e.* 50–400 μg ml^{-1}), on HeLa cells after 6 hours incubation; confocal images (scale bars are 50 μm) show the induced lysosomes (the nucleus and lysosomes are seen as blue and red fluorescence, respectively) and induced ROS level (the nucleus and ROS level are seen as blue and green fluorescence, respectively) obtained by the interactions of HeLa cells with zeolites (concentration of 100 μg ml^{-1}).

the observation on the discrimination between EMT and LTL zeolites may relate to the effect of pore size on the composition of the protein corona. More specifically, the zeolite particles with bigger pores in three-dimensional arrangements have better chance to absorb proteins and nutrition factors from the cell medium, and can cause considerable changes in the cell medium, which in turn can cause false toxicity.[27] In order to check this effect, the modified method[28] using surface saturated zeolites was applied. The results show that the observed differences between the ultra-small EMT and LTL zeolites disappeared (see Fig. 4b). This confirms that the zeolite nanoparticles with a three-dimensional channel system (EMT) are more reactive than the zeolite nanocrystals with one-dimensional channel system (LTL). In addition, the interaction of the zeolites did not cause extensive oxidative stress on the cells (see Fig. 4c). The lysosomes and intracellular ROS of the zeolites (with a concentration of 100 μg ml^{-1}) were visualized by fluorescent microscopy (Fig. 4c). Although the zeolites have extensively entered the cells, there is no sign of toxicity for all employed concentrations of two types zeolite.

Nanoparticles can have a significant effect on the variation of normal cell life cycle.[29,30] The effect of zeolites with various concentrations, on the HeLa cell life cycle at various cycle phases (*i.e.* sub G_0G_1 (apoptotic fraction), G_0G_1 (resting), S (DNA synthesis), and G_2M (mitosis)) was probed. As seen in Fig. 5, the sub G_0G_1 and S phases of the cells interacting with zeolites has been reduced in all tested concentrations. In contrast, the G_0G_1 and G_2M phases have been prolonged after the treatment with zeolites. The reduction in sub G_0G_1 and S areas can reveal the fact that there is no trace of DNA fragmentation and cell apoptosis, even after interaction with a high concentration of zeolites (*i.e.* 400 μg ml^{-1}). Moreover, there are no abnormalities during DNA replication in the presence of zeolite nanoparticles. Therefore, one can expect that the various concentrations of zeolite nanoparticles have negligible effects on the cell life cycle.

Protein corona composition screening and evaluation with ultra-small EMT and LTL zeolites

To screen the corona protein composition in the presence of zeolite nanoparticles, the two types of LTL and EMT zeolite nanoparticles were exposed to human plasma (10% and 100%) for 1 h at room temperature. To remove the unbound proteins from the four samples under study (LTL: LTL-10, LTL-100 and EMT: EMT-10, EMT-100), the samples were five times centrifuged and washed. The plasma of 100% is used since this is the same concentration as an *in vivo* state. The generated peptides derived from the digestion of corona-coated proteins with trypsin were injected into the LC Orbitrap LTQ XL (nLC-tandem MS). The nLC-MS/MS-PEAKS analysis of LTL-corona and EMT-corona samples incubated with human plasma 10% (LTL-10 and EMT-10) reveal 99 and 66 proteins, of which 14 and 7 proteins were found to be shared with LTL-100 and EMT-100, respectively (Fig. 6 and 7, ESI, Tables S1–S4†). Notably, both the LTL- and EMT-corona layers show a high specificity for fibrinogen and a few apolipoproteins such as apoA-I and apoA-II, and low affinity for albumin. Although albumin and IgG constitute approximately 85–90% of human

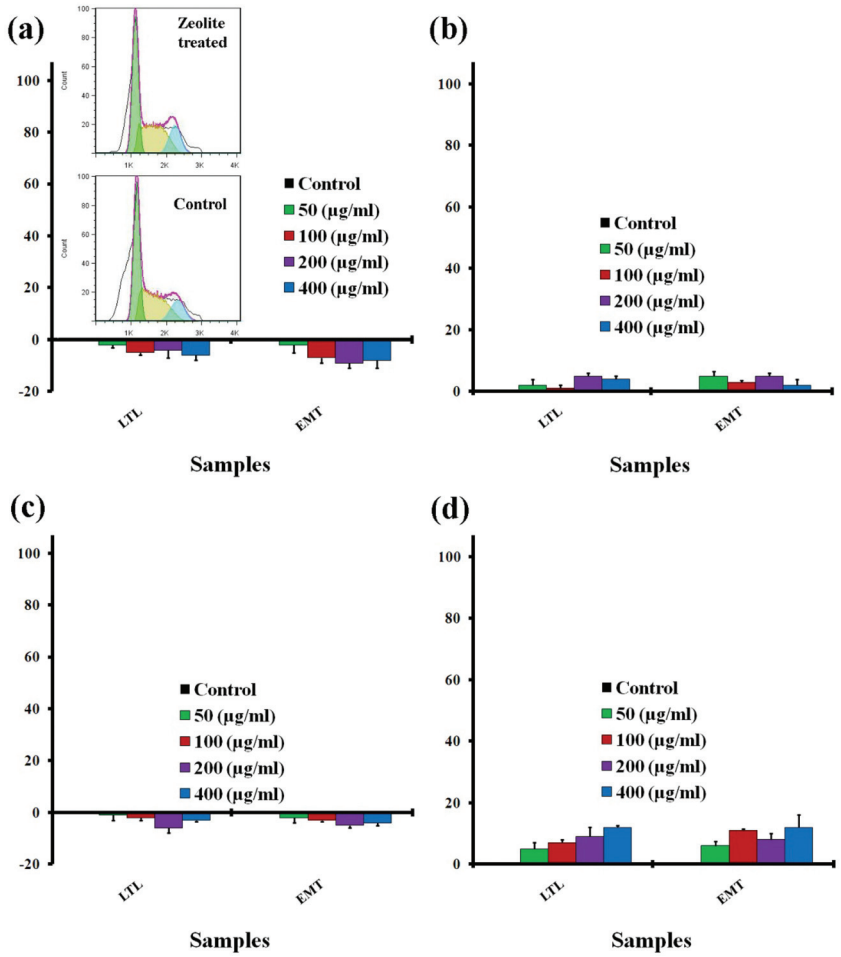

Fig. 5 Cell-life cycle assay results for zeolite-treated HeLa cells showing the percentage of (a) ($subG_0G_1$(control) – $subG_0G_1$(test))/$subG_0G_1$(control), (b) (G_0G_1-(control) – G_0G_1(test))/G_0G_1(control), (c) (S(control) – S(test))/S(control), and (d) (G_2(control) – G_2(test))/G_2(control).

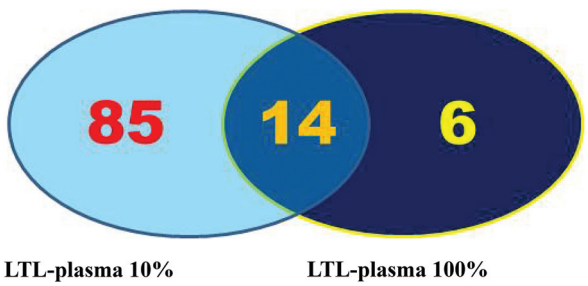

Fig. 6 Comparison between samples LTL-10 and LTL-100; 3 µl injection of peptides derived from trypsin digestion of LTL-corona linked proteins (incubated with 10% human plasma and 100% human plasma) into nLC-MS/MS; generated spectra were analyzed with PEAKS software. False discovery rate (FDR) was manually adjusted to zero. nLC-MS/MS-PEAKS analysis of LTL-10 and LTL-100 lead to the identification of 99 and 20 proteins respectively, of which 14 proteins were found to be present in both states.

plasma proteins, both the LTL- and EMT-type zeolites show a low affinity for these two categories of proteins. On the contrary, both zeolites show high binding capacity for fibrinogen, apoA-I, apoA-II, apoA-IV and apoB (a complex of three different homodimer chains – alpha chain, beta chain and gamma chain); the fibrinogen, apoA-I, apoA-II, apoA-IV and apoB constitute approximately 2–5% of plasma protein composition. However, the specificity of the two types zeolites were highly increased for fibrinogen, apoA-I and apoA-II, and the highest is for fibrinogen. This shows the fact that, during the incubation of the LTL-10 and EMT-10 with proteins, fibrinogen and some of the apolipoprotein-based proteins had higher affinity for binding to the surface of the zeolite nanoparticles as compared to the other proteins. This interpretation is reinforced when the incubation of the LTL-100 and EMT-100 samples is performed; the majority of the corona is occupied by fibrinogen, apolipoproteins, and complement factor 3. Although albumin and IgG are still observed and they are considered as the highest abundant proteins of plasma, the majority of other protein competitors did not bind to the surface (corona layer) of the two types of zeolite. This is due to the high selectivity of the zeolites toward fibrinogen, apolipoproteins, and complement factor 3, and not to their high abundance. Fibrinogen is the most important protein in coagulation cascade and fibrin is an active form of fibrinogen,

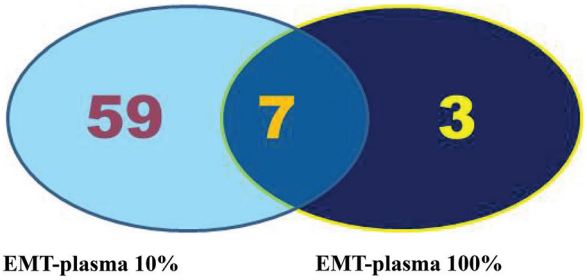

Fig. 7 Comparison between samples EMT-10 and EMT-100; 3 μl injection of peptides derived from trypsin digestion of LTL-corona linked proteins (incubated with 10% human plasma and 100% human plasma) into nLC-MS/MS; generated spectra were analyzed with PEAKS software. False discovery rate (FDR) was manually adjusted to zero. nLC-MS/MS-PEAKS analysis of EMT-10 and ET-100 lead to the identification of 66 and 10 proteins respectively, of which 7 proteins were found to be share.

and both are target of the fibrinolysis system. The current finding could have a great impact in medicine, and in particular in thrombosis and atherothrombosis, which are the latter stage of postcursor of atherosclerosis.

To determine the relative amount of each protein present in corona of samples LTL-10, LTL-100 and EMT-10 and EMT-100, a semi-quantitative approach based on the equation described by Monopoli *et al.* was applied.[23] Eqn (1) is used to calculate $NpSpC_k$ (normalized percentage, Np), where the spectra count (SpC) refers to the protein of interest (k) ($NpSpC_k$), and M_w refers to the molecular weight (kDa) of the protein of interest. $(SpC/M_w)_k$ is the total spectra count for the identified protein of interest divided by its molecular weight in kDa, and $(SpC/M_w)_i$ is the sum of all (SpC/M_w) for each protein per nLC-MS/MS run.

$$NpSpC_k = \left(\frac{(SpC/M_w)_k}{\sum_{i=1}^{n}(SpC/M_w)_i}\right) \times 100 \quad (1)$$

The $NpSpC_k$ values for all proteins identified in the corona of LTL-10, LTL-100, EMT-10 and EMT-100 samples are shown in Tables S1–S4 (ESI†), the $NpSpC_k$ values < 2 for all proteins identified in the corona of LTL-10 and EMT-10 are depicted in Fig. 8 and 9. Additionally, the $NpSpC_k$ values for LTL-100 and EMT-100 are displayed in Fig. 10 and 11. The most striking result is that the relative amount of all three chains of fibrinogen is tremendously higher than other protein competitors such as albumin and IgG in the corona of the two types of zeolites (LTL and EMT). This finding is even more evident for the fibrinogen amount in the corona of the LTL-100 and EMT-100 (Fig. 10–12) than for the LTL-10 and EMT-10 samples (Fig. 8 and 9). The higher specificity (selectivity) of the two samples (LTL-100 and EMT-100) with respect to fibrinogen and apolipoproteins in comparison to samples LTL-10 and EMT-10 is observed. Notably, six proteins are shared, of which three proteins (fibrinogen alpha chain, beta chain and gamma chain) belong to the fibrinogen, one to apoA-II, one to complement factor 3 (CO3) and one to albumin. Therefore it can be concluded that only 4 proteins are shared and not 6, since all three chains of fibrinogen constitute fibrinogen protein. From

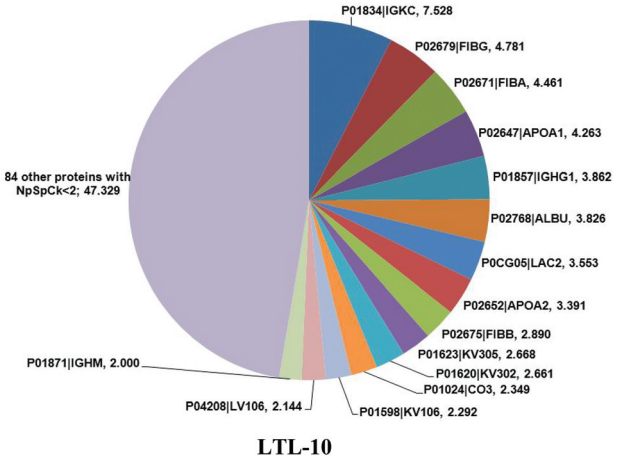

Fig. 8 The $NpSpC_k$ values for all proteins identified in the corona of the LTL-10 sample; protein accession number, gene name, and $NpSpC_k$ values are shown for each protein identified in the corona of the LTL-10 sample. 47.239 is total $NpSpC_k$ for 84 proteins <2.

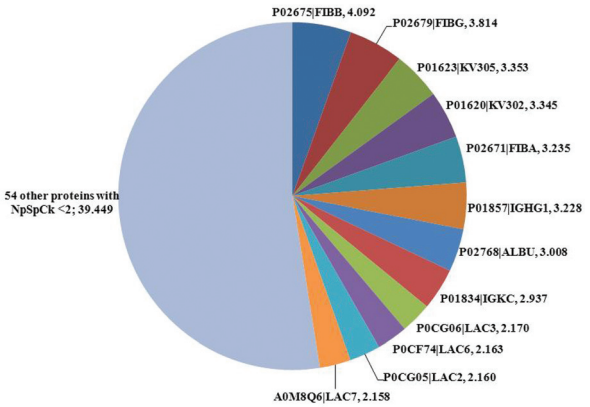

Fig. 9 The $NpSpC_k$ values for all proteins identified in the corona of the EMT-10 sample; protein accession number, gene name, and $NpSpC_k$ values are shown for each protein identified in the corona of the EMT-10 sample. 39.449 is total $NpSpC_k$ for 54 proteins <2.

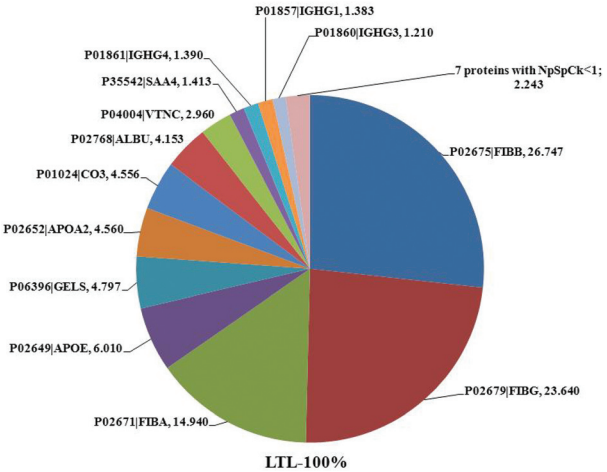

Fig. 10 The $NpSpC_k$ values for all proteins identified in the corona of the LTL-100 sample; the protein accession number, gene name, and $NpSpC_k$ values are shown. 2.243 is total $NpSpC_k$ for 7 proteins <1.

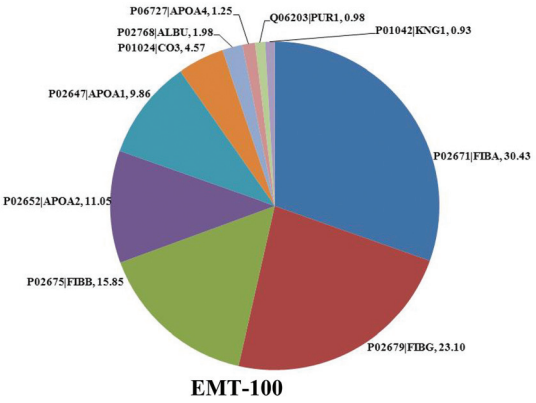

Fig. 11 The $NpSpC_k$ values for all proteins identified in the corona of the EMT-100 sample; the protein accession number, gene name, and $NpSpC_k$ values are shown.

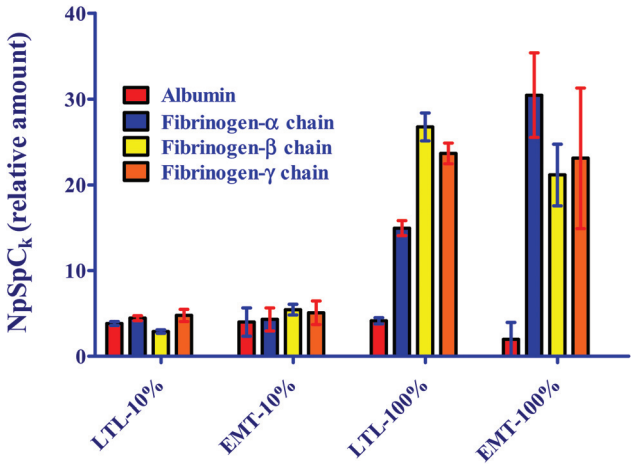

Fig. 13 A comparison of the relative amount of fibrinogen and albumin in samples LTL-10, EMT-10, LTL-100 and EMT-100; the relative amount is shown as $NpSpC_k$. Np is normalized percentage, SpC refers to spectra count per protein and k is protein of interest.

this comparison, it is possible to assume that the corona of EMT-100 is highly specific for fibrinogen and not for albumin, which is the most abundant protein in plasma, but with the lowest $NpSpC_k$ value in the corona of these particles. The share of proteins for LTL-10 and LTL-100, and EMT-10 are presented in Table S5,† while that for EMT-100 is depicted in Table 2. The relative amount of fibrinogen and albumin bound with LTL-10, LTL-100, EMT-10 and EMT-100 nanocrystals is shown in Fig. 13. Importantly, there were no differences between the relative amount of albumin and fibrinogen chains in the samples LTL-10 and EMT-10. However, the relative

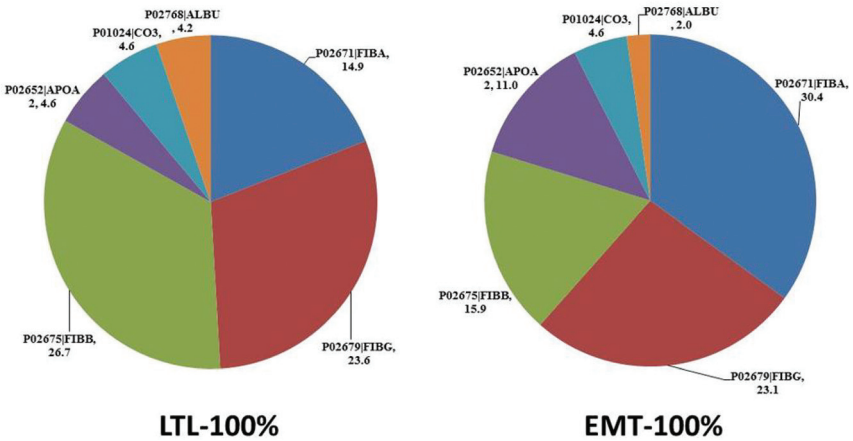

Fig. 12 Shared proteins between samples LTL-100 and EMT-100; protein accession number, gene name and $NpSpC_k$ values are exhibited.

Table 2 The shared proteins identified in samples LTL-100 and EMT-100

				Total spectra		Average $NpSpC_k$	
Accession number	−10 lg P	Mass	Description	LTL-100	EMT-100	LTL-100	EMT-100
P02671|FIBA-HUMAN	257.06	94 973.1	Fibrinogen alpha chain	59	33	14.9	30.4
P02679|FIBG-HUMAN	235.05	51 511.68	Fibrinogen gamma chain	50	12	23.6	23.1
P02675|FIBB-HUMAN	260.4	55 928.21	Fibrinogen beta chain	61	12	26.7	15.9
P02652|APOA2-HUMAN	37.79	11 175.02	Apolipoprotein A-II	2	2	4.6	11.0
P01024|CO3-HUMAN	177.03	187 146.9	Complement C3	34	9	4.6	4.6
P02768|ALBU-HUMAN	147.94	69 366.8	Serum albumin	12	1	4.2	2.0

The accession number, gene name, species (Human), identification score (−10 lg P), molecular weight (M_w) in kDa, protein description, total spectra per protein of LTL and EMT zeolite crystals incubated with 100% human plasma, and the relative amount ($NpSpC_k$ value). The average values are based on four measurements.

amount of fibrinogen is clearly higher as compared to albumin in samples LTL-100 and EMT-100, which indicates that these two types of zeolite nanocrystals have almost no affinity for albumin.

Conclusions

Nanosized EMT- and LTL-type zeolites were synthesized and morphologically characterized, and their cytotoxicity was evaluated. The framework type structure and high micro- and mesoporosity of both zeolites were confirmed by XRD and nitrogen sorption measurements. The sizes and stabilities of the nanosized EMT- and LTL-type crystals were determined by HRTEM/DLS (8–18 nm) and zeta potential characterization (−35 mV). The cytotoxicity was studied by cell viability, ROS and cell life cycle assays. No toxicity was observed for all used zeolite concentrations (100–400 μg ml^{-1}). Although the zeolites can internalize in the cells, fluorescence microscopy confirms the absence of toxicity. Also, the EMT-corona incubated with 100% human plasma shows a very high affinity for fibrinogen and very low affinity for albumin. In conclusion, the zeolite nanoparticles can be considered as very promising materials for purification of fibrinogen and lipoproteins while keeping the same amount of albumin. It is now well recognized that the certain nanoparticles (such as poly(acrylic acid)-coated gold nanoparticles) bind to and induce unfolding of fibrinogen in plasma;[31] the unfolding of fibrinogen may promote interaction with the integrin receptor, Mac-1, leading to the inflammatory responses.[31] Therefore, due to the significant interaction of zeolites with fibrinogen proteins, one can consider these nanoparticles as potential pro-inflammatory agents.

References

1 G. J. D. A. A. Soler-Illia, C. Sanchez, B. Lebeau and J. Patarin, *Chem. Rev.*, 2002, **102**, 4093–4138.
2 M. J. Climent, A. Corma and S. Iborra, *Chem. Rev.*, 2011, **111**, 1072–1133.
3 L. Tosheva and V. P. Valtchev, *Chem. Mater.*, 2005, **17**, 2494–2513.
4 H. Robson, *Microporous Mesoporous Mater.*, 1998, **22**, 525–526.
5 S. Sharifi, S. Behzadi, S. Laurent, M. Laird Forrest, P. Stroeve and M. Mahmoudi, *Chem. Soc. Rev.*, 2012, **41**, 2323–2343.
6 M. Mahmoudi, H. Hofmann, B. Rothen-Rutishauser and A. Petri-Fink, *Chem. Rev.*, 2012, **112**, 2323–2338.
7 R. F. Service, *Science*, 2004, **304**, 1732–1734.
8 L. C. J. Thomassen, D. Napierska, D. Dinsdale, N. Lievens, J. Jammaer, D. Lison, C. E. A. Kirschhock, P. H. Hoet and J. A. Martens, *Nanotoxicology*, 2012, **6**, 472–485.
9 T. Kihara, Y. Zhang, Y. Hu, Q. Mao, Y. Tang and J. Miyake, *J. Biosci. Bioeng.*, 2011, **111**, 725–730.
10 A. Petushkov, J. Intra, J. B. Graham, S. C. Larsen and A. K. Salem, *Chem. Res. Toxicol.*, 2009, **22**, 1359–1368.
11 S. Mintova, N. H. Olson, V. Valtchev and T. Bein, *Science*, 1999, **283**, 958–960.
12 S. Mintova, M. Reinelt, T. H. Metzger, J. Senker and T. Bein, *Chem. Commun.*, 2003, 326–327.
13 B. Z. Zhan, M. A. White, M. Lumsden, J. Mueller-Neuhaus, K. N. Robertson, T. S. Cameron and M. Gharghouri, *Chem. Mater.*, 2002, **14**, 3636–3642.
14 E. P. Ng, D. Chateigner, T. Bein, V. Valtchev and S. Mintova, *Science*, 2012, **335**, 70–73.
15 M. Hölzl, S. Mintova and T. Bein, *Stud. Surf. Sci. Catal.*, 2005, **158**, 1–18.
16 J. L. Casci, *Microporous Mesoporous Mater.*, 2005, **82**, 217–226.
17 H. Wang and J. A. Joseph, *Free Radicals Biol. Med.*, 1999, **27**, 612–616.
18 S. J. Soenen and M. De Cuyper, *Contrast Media Mol. Imaging*, 2011, **6**, 153–164.
19 K. Meijer, M. de Vries, S. Al-Lahham, M. Bruinenberg, D. Weening, M. Dijkstra, N. Kloosterhuis, R. J. van der Leij, H. van der Want, B.-J. Kroesen, R. Vonk and F. Rezaee, *PLoS One*, 2011, **6**, e17154.
20 J. Zhang, L. Xin, B. Shan, W. Chen, M. Xie, D. Yuen, W. Zhang, Z. Zhang, G. A. Lajoie and B. Ma, *Mol. Cell. Proteomics*, 2012, 11.
21 T. Mäurer and B. Kraushaar-Czarnetzki, *Helv. Chim. Acta*, 2001, **84**, 2550–2556.
22 F. Dougnier, J. Patarin, J. L. Guth and D. Anglerot, *Zeolites*, 1992, **12**, 160–166.
23 M. P. Monopoli, D. Walczyk, A. Campbell, G. Elia, I. Lynch, F. Baldelli Bombelli and K. A. Dawson, *J. Am. Chem. Soc.*, 2011, **133**, 2525–2534.
24 M. Mahmoudi, I. Lynch, M. R. Ejtehadi, M. P. Monopoli, F. B. Bombelli and S. Laurent, *Chem. Rev.*, 2011, **111**, 5610–5637.
25 M. P. Monopoli, F. B. Bombelli and K. A. Dawson, *Nat. Nanotechnol.*, 2011, **6**, 11–12.
26 D. Walczyk, F. B. Bombelli, M. P. Monopoli, I. Lynch and K. A. Dawson, *J. Am. Chem. Soc.*, 2010, **132**, 5761–5768.
27 S. Laurent, C. Burtea, C. Thirifays, U. O. Häfeli and M. Mahmoudi, *PLoS One*, 2012, 7.
28 M. Mahmoudi, A. Simchi, M. Imani, M. A. Shokrgozar, A. S. Milani, U. O. Häfeli and P. Stroeve, *Colloids Surf., B*, 2010, **75**, 300–309.
29 M. Mahmoudi, S. N. Saeedi-Eslami, M. A. Shokrgozar, K. Azadmanesh, M. Hassanlou, H. R. Kalhor, C. Burtea, B. Rothen-Rutishauser, S. Laurent, S. Sheibani and H. Vali, *Nanoscale*, 2012, **4**, 5461–5468.
30 M. Mahmoudi, K. Azadmanesh, M. A. Shokrgozar, W. S. Journeay and S. Laurent, *Chem. Rev.*, 2011, **111**, 3407–3432.
31 Z. J. Deng, M. Liang, M. Monteiro, I. Toth and R. F. Minchin, *Nat. Nanotechnol.*, 2011, **6**, 39–44.